GENERAL AND APPLIED PHYSICS

Quantum Metrology for Noisy Systems

B. M. Escher · R. L. de Matos Filho · L. Davidovich

Abstract The estimation of parameters characterizing dynamical processes is a central problem in science and technology. It concerns for instance the evaluation of the duration of some interaction, of the value of a coupling constant, or yet of a frequency in atomic spectroscopy. The estimation error changes with the number N of resources employed in the experiment (which could quantify, for instance, the number of probes or the probing energy). For independent probes, it scales as $1/\sqrt{N}$—the standard limit—a consequence of the central-limit theorem. Quantum strategies, involving for instance entangled or squeezed states, may improve the precision, for noiseless processes, by an extra factor $1/\sqrt{N}$, leading to the so-called Heisenberg limit. For noisy processes, an important question is if and when this improvement can be achieved. Here, we review and detail our recent proposal of a general framework for obtaining attainable and useful lower bounds for the ultimate limit of precision in noisy systems. We apply this bound to lossy optical interferometry and show that, independently of the initial states of the probes, it captures the main features of the transition, as N grows, from the $1/N$ to the $1/\sqrt{N}$ behavior.

1 Introduction

The estimation of parameters is an essential part of the scientific analysis of experimental data. It plays an important role at a very basic level, involving the measurement of fundamental constants of Nature—as for instance the Planck constant, the fine structure constant, the speed of light in vacuum, and the gravitational constant. Furthermore, it has widespread practical implications in the characterization of parameter-dependent physical processes. Examples are easy to find. Petrobras, the Brazilian oil company, estimates the characteristics of a subsalt oil deposit through the scattering of seismic waves, robotic engineers may want to scan a photographic image to estimate the position and orientation of an object, physicists wish to estimate the transition frequency or the lifetime of an atom, or yet the phase shift in an interferometric measurement, due to the presence of gravitational waves.

Detailed techniques for parameter estimation, dating back to the work of Fisher [1, 2], Cramér [3], and Rao [4], have allowed the characterization of the achievable limits in the precision of estimation.

The basic steps in parameter estimation are illustrated in Fig. 1. A probe, prepared in a known initial configuration, is sent through the parameter-dependent process to be investigated; the final configuration of the probe is measured, and from this measurement one estimates the value of the parameter.

Since realistic experimental data have statistical uncertainties, due to external perturbations, intrinsic fluctuations, or imperfect detectors, it is not possible to biunivocally associate an experimental result (through an estimation) with the true value of the parameter. The error in an estimation may be quantified by the square root of the statistical average of the square of the difference between the estimated and the true value of the parameter. The so-called Cramér–Rao limit (see Section 2) yields a lower bound to this error, which is

B. M. Escher (✉) · R. L. de Matos Filho ·
L. Davidovich
Instituto de Física, Universidade Federal do Rio de Janeiro,
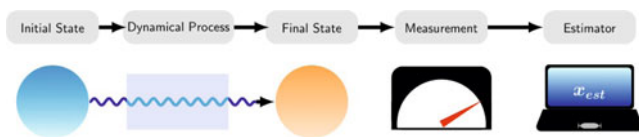21941-972, Rio de Janeiro (RJ), Brazil
e-mail: bmescher@if.ufrj.br

Fig. 1 (Color online) General setup for parameter estimation. A probe, prepared in a known initial state (first sphere on the left), is sent through the parameter-dependent process to be investigated; the final configuration is measured, the outcome of this measurement being then used to estimate the value of the parameter

inversely proportional to the square root of the number ν of repetitions of the measurement process. In single-parameter estimation, this bound is expressed in terms of a quantity known as Fisher Information, to be defined later in this article (Section 2): the larger this quantity, the more accurate can the estimation be.

The Fisher information may be considered as a measure of the maximum amount of information that can be extracted from experiments about the true value of an unknown parameter [3, 4]. This quantifier of information depends on properties of the probe, the parameter-dependent process, and the measurement on the probe used to investigate the process. An important aim of metrology is to calculate the Fisher Information, to find ways to maximize it, and to find protocols that allow for better estimation.

Quantum Metrology [5, 6] also deals with parameter estimation but takes into account the quantum character of the systems and processes involved. In this case, the estimation error is still limited by the Cramér–Rao bound, expressed in terms of the Fisher Information, which as before quantifies the maximum amount of information that can be extracted about the parameter, considering however the constraints imposed by quantum physics; in particular, its intrinsic probabilistic nature, the dependence of the result on the measurement scheme, and the more restricted set of possible measurements.

The so-called Quantum Fisher Information [7] is defined by maximizing the Fisher information over all possible measurement strategies allowed by quantum mechanics. It characterizes the maximum amount of information that can be extracted from quantum experiments about an unknown parameter using the best (and ideal) measurement device. It establishes the best precision that can be attained with a given quantum probe. The ultimate precision limit in quantum parameter estimation is obtained by further maximizing the Quantum Fisher Information over all initial states of the probe. In the ideal situation of systems isolated from the environment, useful analytic results allow the

calculation of this ultimate bound. It can be shown then that quantum strategies, involving non-classical characteristics of the probes, like entanglement and squeezing, lead to much better bounds, as compared with standard approaches that do not profit from these properties [8]. Thus, for instance, in optical interferometry, the determination of a phase as a function of the number N of photons, scales with $1/\sqrt{N}$ in the standard limit, while entangled N-photon states lead to a scaling proportional to $1/N$, leading therefore to a better resolution for the same amount of resources.

The quantum theory of parameter estimation allows a useful complementation of the Heisenberg inequalities, associated with Hermitian operators and their canonical conjugates. Quantum Metrology leads to inequalities involving parameters and operators, instead of just operators, thus allowing for instance a precise formulation of the time-energy and the phase-number uncertainty relations.

Until recently, most of the work in Quantum Metrology involved isolated systems undergoing unitary evolutions. However, systems cannot be completely isolated from their environments. This leads to extra fluctuations and the phenomenon of decoherence, which counteracts quantum effects, thus limiting the usefulness of quantum strategies. In particular, entangled states are known to be very sensitive to the action of the environment [9–11]. It is, therefore, important to establish the robustness of quantum strategies. Unfortunately, the determination of the ultimate precision bound for systems under the influence of the environment usually involves hard numerical work [12, 13] since there has been up to now no general approach for this more realistic situation [14, 15].

In a recent paper [16], we have proposed a general framework for quantum metrology of noisy systems. It was shown to lead to useful analytic bounds for important problems, like optical interferometry and atomic spectroscopy. In the present article, we review some of the results obtained in that publication, and give further details on the method.

The main idea behind the proposed approach is to consider the probe together with an environment as a single entity and to consider the Quantum Fisher Information corresponding to this enlarged system, which implies a maximization over all possible measurement strategies applied to the ensemble probe plus environment. This quantity is, then, an upper bound to the Quantum Fisher Information of the probe alone. It can be shown that there are several (in fact, infinite!) equivalent environments that lead to the same noisy dynamics of the probe. In Ref. [16], it was demonstrated however that it is always possible to choose

an environment so that the information about the parameter, obtained from measurements on the probe plus environment, is redundant with respect to the information obtained from the probe alone. In this case, the Quantum Fisher Information of the enlarged system coincides with the corresponding quantity for the probe. This allows in principle the determination of the ultimate precision limit by using the methods previously developed for isolated systems.

Even though finding this special class of environment is in general a difficult problem, useful approximations, based on physical insights, can be found, which yield analytical bounds for the precision in noisy systems. This method was applied in [16] to lossy optical interferometry and atomic spectroscopy under dephasing, elucidating in both cases how noise affects the precision in the estimation of the relevant parameter. Thus, for a noisy optical interferometer, probed by N photons, it was shown that there is a continuous transition of the precision in the estimation of phase shifts, as the number of photons increases, from a $1/N$ scaling, the ultimate quantum limit in the absence of noise, to the so-called standard limit, inversely proportional to $1/\sqrt{N}$. This result shows that noise leads unavoidably to the standard limit scaling, as the number of photons reaches a critical value, which depends on the noise strength.

In this paper, we review the main results of the general theory of parameter estimation and detail the work on optical interferometry presented in [16]. In Section 2, we derive the classical Cramér–Rao bound. The problem of quantum parameter estimation is introduced in Section 3, where we discuss its relation to the distinguishability between quantum states. The generalization of the Cramér–Rao bound to quantum mechanics is presented in Section 4, and the special case of pure states undergoing unitary evolution, which leads to simple analytical expressions for the precision bound, is discussed in Section 5. Some examples are discussed in Section 6, where it is shown that the quantum Cramér–Rao bound allows a precise formulation of the time energy and phase-number uncertainty relations, and has an important application to optical interferometry. Section 7 deals with the problem of parameter estimation with decoherence, which implies a strong change in the scenario previously described for pure states. It reviews recent experiments in optical interferometry that investigate the effects of noise on the ultimate limits of precision, and introduces a general framework for obtaining useful precision bounds for noisy quantum-enhanced metrology. This general result is applied to optical interferometry in Section 8, where it leads to an analytical bound that continuously interpolates between the Heisenberg and the standard scaling. Section 9 contains a brief review of nonlinear estimation strategies, which help to reduce uncertainties beyond the Heisenberg limit. Our conclusions are summarized in Section 10.

2 Parameter Estimation: The Cramér–Rao Bound

We discuss now in detail the general approach to parameter estimation, as initiated by Cramér and Rao. The aim is to estimate the value of a parameter x, following the steps described in Fig. 1. We denote by x_{true} the true value of the parameter.

A convenient merit quantifier is defined by

$$\sigma \equiv \sqrt{\langle [x_{\text{est}} - x_{\text{true}}]^2 \rangle}, \tag{1}$$

where x_{est} is the estimated value of the parameter for a possible measurement result, x_{true} is the true value of the parameter, and the average indicated by the brackets $\langle \rangle$ is taken over all measurement results .

Cramér and Rao established a bound for unbiased estimators [3, 4]—to be defined later in this section. They showed that the standard deviation in the estimation is bounded below by a quantity inversely proportional to the square root of the number of samplings ν,

$$\sigma \geqslant \frac{1}{\sqrt{\nu F(x_{\text{true}})}}, \tag{2}$$

where the function $F(x)$, known as the *Fisher information*, is given for a discrete set of measurement results by

$$F(x) \equiv \sum_j p_j(x) \left(\frac{d \ln [p_j(x)]}{dx} \right)^2. \tag{3}$$

Here, $p_j(x)$ is the probability of getting an experimental result j, given that the parameter is x. For a continuum set of results, (3) generalizes to:

$$F(x) \equiv \int d\xi \, p(\xi|x)) \left(\frac{\partial \ln p(\xi|x)}{\partial x} \right)^2, \tag{4}$$

where $p(\xi|x)d\xi$ is the probability of finding the experimental result between ξ and $\xi + d\xi$.

We derive now the Cramér–Rao bound (2). The goal is to estimate a real parameter x, which could be single or multivariate. To be specific, we consider a single continuous parameters and ν identical measurements.

Let $\xi_1, \xi_2, \ldots, \xi_\nu$ be the results of the ν measurements and let $p(\xi|x)$ be the probability density to have the result ξ, given that the parameter is x. We estimate the parameter x by means of a function

$$x_{\text{est}} = x_{\text{est}}(\xi_1, \ldots, \xi_\nu), \tag{5}$$

constructed from the ν results ξ_i $(i = 1, \ldots, \nu)$ with an appropriate algorithm. The function x_{est} depends on the ξ_i $(i = 1, \ldots, \nu)$, not on the unknown parameter x.

We start out with the following, trivial identity:

$$\int \mathrm{d}\xi_1 \ldots \mathrm{d}\xi_\nu \, p(\xi_1|x) \ldots p(\xi_\nu|x) \, \Delta x_{\text{est}} = 0, \tag{6}$$

where

$$\Delta x_{\text{est}} = x_{\text{est}}(\xi_1, \ldots, \xi_\nu) - \langle x_{\text{est}} \rangle_x, \tag{7}$$

the index x being used to remind one that the averaged estimate depends on x. The product in the integrand on the left-hand side of (6) is the probability density $P(\xi_1, \ldots, \xi_\nu|x)$ that ν measurements of x yield the results $\xi_1, \ldots, \xi_\nu$, i.e.,

$$P(\xi_1, \ldots, \xi_\nu|x) = p(\xi_1|x) \ldots p(\xi_\nu|x), \tag{8}$$

because we are dealing with independent measurements. The integral must therefore vanish, since

$$\int \mathrm{d}\xi_1 \ldots \xi_\nu \, x_{\text{est}} \, P(\xi_1, \ldots, \xi_\nu|x) = \langle x_{\text{est}} \rangle_x. \tag{9}$$

We next differentiate both sides of (6) with respect to x, keeping in mind that, while $x_{\text{est}}(\xi_1, \ldots, \xi_\nu)$ is independent of the parameter x, the average $\langle x_{\text{est}} \rangle$ is not, because the probability densities $p(\xi|x)$ depend on x. The result is the equality

$$\frac{d\langle x_{\text{est}} \rangle_x}{\mathrm{d}x} = \int \mathrm{d}\xi_1 \ldots \mathrm{d}\xi_\nu \, \Delta x_{\text{est}}(\xi_1, \ldots, \xi_\nu) \tag{10}$$

$$\times \sum_{n=1}^{\nu} \frac{p(\xi_1|x) \ldots p(\xi_\nu|x)}{p(\xi_n|x)} \frac{\partial p(\xi_n|x)}{\partial x},$$

equivalent to the expression

$$\frac{d\langle x_{\text{est}} \rangle_x}{\mathrm{d}x} = \int \mathrm{d}\xi_1 \ldots \mathrm{d}\xi_\nu \, p(\xi_1|x) \ldots p(\xi_\nu|x)$$

$$\times \left(\sum_{n=1}^{\nu} \frac{\partial \ln p(\xi_n|x)}{\partial x} \right) \Delta x_{\text{est}}(\xi_1, \ldots, \xi_\nu). \tag{11}$$

The right-hand side of (11) can be regarded as a scalar product between the vectors $\{\partial \ln p(\xi_1|x)/ \partial x, \ldots, \partial \ln p(\xi_\nu|x)/\partial x\}$, and $\{\Delta x_{\text{est}}, \ldots, \Delta x_{\text{est}}\}$, the product of the probability densities $p(\xi_1|x) \ldots p(\xi_\nu|x)$

being the measure. To this scalar product, we can apply the Schwarz inequality, which reads

$$\langle (\Delta x_{\text{est}})^2 \rangle \int \mathrm{d}\xi_1 \ldots \mathrm{d}\xi_\nu \, p(\xi_1|x) \ldots p(\xi_\nu|x)$$

$$\times \left(\sum_{n=1}^{\nu} \frac{\partial \ln p(\xi_n|x)}{\partial x} \right)^2 \geqslant \left(\frac{d\langle x_{\text{est}} \rangle_x}{\mathrm{d}x} \right)^2. \tag{12}$$

Inspection of the squared sum in the integrand on the left-hand side shows that the cross terms vanish, since

$$\int \mathrm{d}\xi_i \, p(\xi_i|x) \frac{\partial \ln p(\xi_i|x)}{\partial x} = \int \mathrm{d}\xi_i \, \frac{\partial p(\xi_i|x)}{\partial x}$$

$$= \frac{d}{\mathrm{d}x} \int \mathrm{d}\xi_i \, p(\xi_i|x), \tag{13}$$

and hence equals zero.

Without the cross terms in the squared sum on the left-hand side, (12) reduces to

$$\langle (\Delta x_{\text{est}})^2 \rangle \int \mathrm{d}\xi_1 \ldots \mathrm{d}\xi_\nu \, p(\xi_1|x) \ldots p(\xi_\nu|x)$$

$$\sum_{n=1}^{\nu} \left(\frac{\partial \ln p(\xi_n|x)}{\partial x} \right)^2 \geqslant \left(\frac{d\langle x_{\text{est}} \rangle_x}{\mathrm{d}x} \right)^2, \tag{14}$$

which can equally well be written in the form

$$\langle (\Delta x_{\text{est}})^2 \rangle \sum_{n=1}^{\nu} \int \mathrm{d}\xi_1 \ldots \mathrm{d}\xi_\nu \, p(\xi_1|x) \ldots p(\xi_\nu|x)$$

$$\times \left(\frac{\partial \ln p(\xi_n|x)}{\partial x} \right)^2 \geqslant \left(\frac{d\langle x_{\text{est}} \rangle_x}{\mathrm{d}x} \right)^2. \tag{15}$$

The summand on the left-hand side is the product of ν factors. $\nu - 1$ of these are integrals of the form $\int \mathrm{d}\xi_i \, p(\xi_i|x)$ $(i = 1, \ldots, n-1, n+1, \ldots, \nu)$, each of which equals unity. The remaining factor is the integral

$$F(x) = \int \mathrm{d}\xi_n \, p(\xi_n|x) \left(\frac{\partial p(\xi_n|x)}{\partial x} \right)^2, \tag{16}$$

which is independent of n. The inequality (15) is therefore equivalent to the expression

$$\langle (\Delta x_{\text{est}})^2 \rangle \nu F(x) \geqslant \left(\frac{d\langle x_{\text{est}} \rangle_x}{\mathrm{d}x} \right)^2, \tag{17}$$

which can be written in the form

$$\frac{\langle (\Delta x_{\text{est}})^2 \rangle}{(d\langle x_{\text{est}} \rangle_x/\mathrm{d}x)^2} \geqslant \frac{1}{\nu F(x)}. \tag{18}$$

Equation (16) coincides with the definition (4) of the Fisher information. Nonetheless, (18) is still somewhat

distant from the result we want, because here the deviation Δx_{est}, defined by (7), is measured with respect to the average value $\langle x_{\text{est}} \rangle_x$ of the estimation, not with respect to the real value of the parameter.

We want to know how close we are to the real value. To this end, we examine the difference

$$\delta x \equiv \frac{x_{\text{est}}}{|d\langle x_{\text{est}} \rangle_x / dx|} - x, \tag{19}$$

a definition calling for a brief digression. One might argue that, instead of the right-hand side of (19), the relevant difference is $x_{\text{est}} - x$. And so we have to justify the derivative in the denominator of the first term on the right-hand side.

There are two reasons for this derivative. One of them has to do with dimensions or units. Suppose that one is interested in the explosion of a bomb. A succession of movie frames is recorded at very fast rate. When the movie is projected at a slower rate, details of the process become visible, but of course a price must be paid: the time intervals have to be scaled. The derivative on the right-hand side of (19) accounts for the change of units (or, more generally, of dimensions).

And there is a second reason. Suppose that instead of working hard to measure the parameter, a student decides to make wild guesses. Instead of reading the appropriate meter, the student records a value V, which may or may not be close to the real value. In any event, the wild guesses should be penalized. And in fact, since the values V are independent of the measurement, their average is independent of x, the derivative $d\langle x_{\text{est}} \rangle_x / dx$ is zero, and the uncertainty on the right-hand side of (19) is infinite. We see that the derivative in the denominator on the right-hand side not only corrects for the units; it also punishes wild guesses. The definition in (19), which turns out to be convenient for several purposes, was introduced by Braunstein and Caves [7].

When both sides of (19) are squared and averaged, the following expression results for the standard deviation:

$$\langle (\delta x)^2 \rangle = \frac{\langle (\Delta x_{\text{est}})^2 \rangle}{(d\langle x_{\text{est}} \rangle_x / dx)^2} + \langle \delta x \rangle^2, \tag{20}$$

where the quantity squared in the second term on the right-hand side is the average of the uncertainty defined by (19).

In view of the inequality (18), we therefore have that

$$\langle (\delta x)^2 \rangle \geqslant \frac{1}{\nu F(x)} + \langle \delta x \rangle^2. \tag{21}$$

The second term on the right-hand side is positive whenever the average of the first term on the right-hand side of (19) differs from x.

In the case of unbiased estimators, defined so that the average $\langle x_{\text{est}} \rangle_x$ is equal to x, the derivative $d\langle x_{\text{est}} \rangle_x / dx$ is equal to one, $\langle \delta x \rangle = 0$, and inequality (21) reduces to

$$\langle (\delta x)^2 \rangle = \langle (\Delta x)^2 \rangle \geqslant \frac{1}{\nu F(x)}. \tag{22}$$

For $x = x_{\text{true}}$, $\sqrt{\langle (\delta x)^2 \rangle}$ coincides with σ defined by (1), and one gets therefore from the above equation the Cramér–Rao bound for unbiased estimators (1).

We see that the derivation of (22) relies on statistical concepts only. The bound follows from simple mathematics and general considerations concerning the distribution probability for the sequence of ν measurements.

Fisher showed that inequality (22) can be saturated asymptotically when $\nu \to \infty$, i.e., that it is possible to choose an appropriate estimator (obtained through maximum likelihood) so that

$$\sigma = \frac{1}{\sqrt{\nu F(x_{\text{true}})}}. \tag{23}$$

We say that the right-hand side is an attainable bound. And if the Fisher information $F(x)$ is independent of ν, the equality implies $1/\sqrt{\nu}$ behavior for σ. This result follows from (8), i.e., from the assumption that the measurements are independent events.

3 Quantum Parameter Estimation

We now turn to quantum mechanics and follow the same reasoning. A probe is sent through a parameter-dependent dynamical process, the final state is measured, and the parameter is estimated from the result. An important contribution to our understanding of this problem was provided by Braunstein and Caves [7] who associated the accuracy in the estimation to a fundamental quantum concept: the distinguishability between two states.

To be specific, we consider an example from optical interferometry. Figure 2 shows a Mach–Zehnder interferometer [8], with a beam splitter, two sets of two mirrors and, between them, a sample that introduces a phase displacement θ in one of the arms of the interferometer. From the outcome, the displacement θ is estimated. The standard limit, obtained when independent photons (for instance, in a coherent state) are sent through the interferometer, leads to

$$\delta\theta \propto \frac{1}{\sqrt{\nu \langle n \rangle}}, \tag{24}$$

where $\langle n \rangle$ is the average number of photons in the field.

It is easy to interpret (24), if the phase is probed with coherent states. Suppose that there is no phase displacement when a coherent state is sent through the pertinent arm of the interferometer, and then there is a phase fluctuation $\delta\theta$, after which a second coherent state is sent through the same arm. The second coherent state will have a displaced phase with respect to the first one, due to the fluctuation $\delta\theta$.

We will be able to detect the change in phase if the second coherent state, $|\alpha e^{i\delta\theta}\rangle$, is distinguishable from the first one, $|\alpha\rangle$. If the two states overlap strongly, detection will be impossible. Detecting the phase displacement is hence equivalent to distinguishing the state $|\alpha\rangle$ from $|\alpha e^{i\delta\theta}\rangle$.

If $\delta\theta$ is small, the overlap between the two states can be approximately written in the form

$$\left|\langle\alpha|\alpha e^{i\delta\theta}\rangle\right|^2 = \exp\left(-\left|\alpha(1-e^{i\delta\theta})\right|^2\right) \approx \exp\left[-\langle n\rangle(\delta\theta)^2\right]. \tag{25}$$

We conclude that the overlap between the two coherent states becomes small when $\langle n\rangle(\delta\theta)^2$ is of the order of unity, in agreement with (24).

Given the simplicity of the argument leading to (25), one might infer that the right-hand side of (24) is an absolute lower bound. Smaller uncertainties nonetheless result when entangled states are substituted for the coherent ones. To see that, consider the NOON state [17, 18]

$$|\psi(N)\rangle = \frac{|N,0\rangle + |0,N\rangle}{\sqrt{2}}. \tag{26}$$

The quantum states in the numerator on the right-hand side have N photons in one of the arms of the interferometer and none in the other, the coherent superposition of the two states indicating that we do not know if the N photons are in the upper or the lower arm.

Suppose we send a NOON state through the interferometer, balanced in such a way that the phase difference between the upper and the lower arm is zero. For a phase fluctuation $\delta\theta$ in the upper arm, the state with N photons in this arm will acquire a phase factor $e^{iN\delta\theta}$, because the displacement is proportional to the number of photons in the arm. The outgoing NOON state is

$$|\psi(N,\delta\theta)\rangle = \frac{e^{iN\delta\theta}|N,0\rangle + |0,N\rangle}{\sqrt{2}}. \tag{27}$$

To determine the phase displacement $\delta\theta$ that makes the final state orthogonal to the initial one, which will

define the resolution of the experiment, we compute the scalar product between the initial and the final states:

$$|\langle\psi(N)|\psi(N,\delta\theta)\rangle|^2 = \cos^2(N\delta\theta/2), \tag{28}$$

which vanishes for $N\delta\theta = \pi$, i.e., for

$$\delta\theta \approx \frac{1}{N}. \tag{29}$$

Comparison with (24) shows that, with the same number of photons, i.e., with the same resources, the NOON state yields more precise results than coherent states.

Let us now look at the problem of quantum parameter estimation from a broader perspective [5, 6], as illustrated in Fig. 3. We consider an initial state $|\psi\rangle$ and a trace-preserving physical process dependent upon a parameter x. We call this dynamical process a *quantum channel*. When the state is sent through the channel, a density matrix $\hat\rho(x)$ results. Detection follows and yields an estimate of the parameter x embedded in the physical process.

If the evolution is unitary, then the density matrix of the probe at the end of the first step of the process (before measurement) is given by

$$\hat\rho(x) = \hat{U}(x)\hat\rho\hat{U}^\dagger(x), \tag{30}$$

where $\hat{U}(x)$ is the evolution operator corresponding to the physical process and $\hat\rho$ is the initial density operator of the probe.

If, on the other hand, the process is non-unitary, (30) is no longer valid, but we can still write a similar expression, of the following form:

$$\hat\rho(x) = \sum_i \hat\Pi_i(x)\hat\rho\hat\Pi_i^\dagger(x), \tag{31}$$
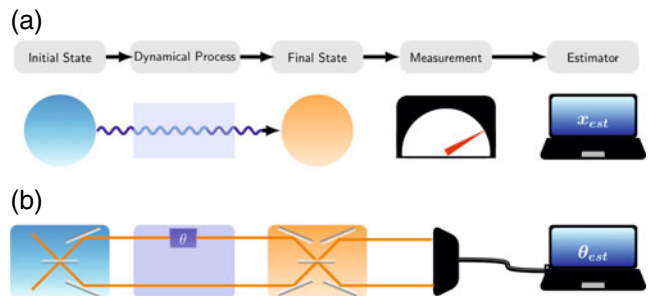
(a)

(b)

Fig. 2 (Color online) Setups for quantum parameter estimation. **a** General setup: a probe prepared in a known initial state is sent through a parameter-dependent physical process, the final state of the probe is measured, and from the results of the measurement one estimates the value of the parameter. **b** Setup for estimating a phase θ in a Mach–Zehnder interferometer

where the operators $\hat{\Pi}_i(x)$, known as the Kraus operators [19], satisfy the condition

$$\sum_i \hat{\Pi}_i^\dagger(x)\hat{\Pi}_i(x) = \mathbb{1}. \tag{32}$$

One can regard (31) as the integral version of the master equation for the system.

In the second step, we have to choose a suitable measurement, and in quantum mechanics, this amounts to associating a set of Hermitian operators $\hat{E}_j$ with the measurement. The latter are *Positive-Operator Valued Measures* (POVM), a generalization of the von-Neumann projection operators [20], since they do not correspond necessarily to orthogonal measurements. In particular, the $\hat{E}_j$ should add up to the identity operator,

$$\sum_j \hat{E}_j = \mathbb{1}, \tag{33}$$

and are such that the probability of obtaining an experimental result j, if the value of the parameter is x, is given by

$$p_j(x) = \mathrm{Tr}\left[\hat{\rho}(x)\hat{E}_j\right]. \tag{34}$$

In the continuous case, we have to substitute a continuous variable ξ for the index j, so that $\hat{E}_j \rightarrow \hat{E}(\xi)$, an integral for the sum on the left-hand side of (33),

$$\int \mathrm{d}\xi \, \hat{E}(\xi) = 1, \tag{35}$$

and the following expression for (34):

$$p(\xi|x) = \mathrm{Tr}\left[\hat{\rho}(x)\hat{E}(\xi)\right]. \tag{36}$$

This is the quantum mechanical version of the procedure in Section 2.

Next, in the third step, with each experimental result j, which corresponds to the operator $\hat{E}_j$, we associate an estimation $x_{\mathrm{est}}(j)$.

Finally, we have to estimate the merit of the estimation. To this end, as before, we apply the merit quantifier based on (19), which yields, for unbiased estimators,

$$\sqrt{\langle (\delta x)^2 \rangle} = \sqrt{\langle (x_{\mathrm{est}} - x)^2 \rangle}. \tag{37}$$

The quantum and classical procedures are very similar. The noteworthy difference is (36), which relates the probabilities to the POVMs $\hat{E}_j$ and depends on the density matrix of the system after undergoing the dynamical process.

4 Quantum Cramér–Rao Bound

We can now derive a quantum Cramér–Rao bound. We follow the steps in Section 3, notice taken that the probability density associated with the result ξ, for given parameter x, is now determined by (36) and that the non-negative Hermitian operators $\hat{E}(\xi)$ are subject to the condition (35). For an unbiased estimator, the calculation in Section 3 then shows that the variance is subject to the bound we have found before:

$$\sqrt{\langle (\delta x)^2 \rangle} \geqslant \frac{1}{\sqrt{\nu F(x)}}, \tag{38}$$

where δx is given by (19) with $d\langle x_{\mathrm{est}}\rangle_x / dx = 1$, that is, $\delta x = x_{\mathrm{est}} - x$, and the Fisher information is

$$F(x) = F\left[x; \{\hat{E}(\xi)\}\right] = \int \mathrm{d}\xi \, p(\xi|x)\left[\frac{\partial \ln p(\xi|x)}{\partial x}\right]^2, \tag{39}$$

which can also be written as

$$F(x) = \int \mathrm{d}\xi \, \frac{1}{p(\xi|x))}\left[\frac{\partial p(\xi|x)}{\partial x}\right]^2. \tag{40}$$

An additional step is now necessary. The bound in (40) reflects an optimization over estimators for a given quantum measurement, as Fisher's argument shows; the best estimator attains the bound. As discussed in Section 3, Fisher's concepts were initially developed with classical systems in mind. In quantum theory, the experimental strategy matters, and we should hence optimize the procedure over all quantum measurements. This leads to the *quantum Fisher information*, defined by

$$\mathcal{F}_Q(x) \equiv \max_{\{\hat{E}(\xi)\}} F\left[x; \{\hat{E}(\xi)\}\right], \tag{41}$$

and the quantum Cramér–Rao bound reads

$$\sqrt{\langle (\delta x)^2 \rangle} \geqslant \frac{1}{\sqrt{\nu \mathcal{F}_Q(x)}}. \tag{42}$$

In the quantum case, we can take advantage of the freedom to choose the experimental setup to optimize the bound.

5 Quantum Fisher Information for Pure States

At this point, one may ask whether explicit expressions can be obtained for the quantum Fisher information, i.e., for the right-hand side of (41). At first sight, it may seem very difficult to write one such expression, given that we have to find the ideal estimator and

then optimize over all possible measurements. Such obstacles notwithstanding, in the case of pure states and unitary processes a simple, exact expression has been derived. As shown in [7], the Fisher information is proportional to the variance of an operator $H(x)$ associated with the unitary evolution by the expression

$$\hat{H}(x) = i \frac{d\hat{U}^{\dagger}(x)}{\mathrm{d}x} \hat{U}(x). \tag{43}$$

$\hat{H}(x)$ is the generator of the transformation associated with the parameter x. In fact, if

$$\hat{U}(x) = \exp(i\hat{O}x), \tag{44}$$

where the operator $\hat{O}$ is independent of x, then $\hat{H} = \hat{O}$.

More explicitly, in the unitary case, for a pure system, the quantum Fisher information is given by the simple expression

$$\mathcal{F}_Q(x) = 4\langle(\Delta\hat{H})^2\rangle_0, \tag{45}$$

where

$$\langle(\Delta\hat{H})^2\rangle_0 \equiv \langle\psi_0|\left(\hat{H}(x) - \langle\hat{H}(x)\rangle_0\right)^2|\psi_0\rangle \tag{46}$$

and the index 0 indicates an average over the initial state of the probe $|\psi_0\rangle$. Therefore, in this case,

$$\sqrt{\langle(\delta x)^2\rangle} \geqslant \frac{1}{2\sqrt{\nu\langle(\Delta\hat{H})^2\rangle_0}}. \tag{47}$$

In the pure, unitary case, therefore, to maximize the Fisher information, which is the same as minimizing the Cramér–Rao bound, we have to maximize the right-hand side of (46). In brief, to optimally improve the precision we first have to identify the generator of the transformation associated with the parameter under study and then we must find a state that maximizes the variance of the generator.

Equation (47) was named a "generalized uncertainty relation" in [21]. As opposed to the usual uncertainty relations in quantum mechanics, it does not relate the variance of two operators, but instead the variances of a parameter and an operator.

We now present a simple derivation of (45).

Let us consider a unitary process, such that the initial state of the probe is $|\psi_0\rangle$, and the final x-dependent state is $|\psi(x)\rangle = \hat{U}(x)|\psi_0\rangle$, where $\hat{U}(x)$ is a unitary operator. Define $\hat{h}(x) \equiv -i\frac{d\hat{U}(x)}{\mathrm{d}x}\hat{U}^{\dagger}(x)$, so that $\frac{d|\psi(x)\rangle}{\mathrm{d}x} = i\hat{h}(x)|\psi(x)\rangle$.

Let $p(\xi|x) = \langle\psi(x)|\hat{E}(\xi)|\psi(x)\rangle$, $\int d\xi\, \hat{E}(\xi) = \mathbf{1}$, where $\hat{E}(\xi)$ stands for a set of POVM's corresponding to a measurement made on the probe, and ξ are the corresponding experimental results. Then

$$\frac{\partial p(\xi|x)}{\partial x} = \left[\frac{d}{\mathrm{d}x}\langle\psi(x)|\right]\hat{E}(\xi)|\psi(x)\rangle$$
$$+ \langle\psi(x)|\hat{E}(\xi)\left[\frac{d}{\mathrm{d}x}|\psi(x)\rangle\right]$$
$$= i\langle\psi(x)|[\hat{E}(x), \hat{h}(x)]|\psi(x)\rangle$$
$$= -2\mathrm{Im}\left[\langle\psi(x)|\hat{E}(x)\hat{h}(x)|\psi(x)\rangle\right], \tag{48}$$

which may also be written as [with $g(x)$ an arbitrary real function]:

$$\frac{\partial p(\xi|x)}{\partial x} = -2\mathrm{Im}\left\{\langle\psi(x)|\hat{E}(x)\left[\hat{h}(x) - g(x)\right]|\psi(x)\rangle\right\}. \tag{49}$$

Therefore,

$$\left[\frac{\partial p(\xi|x)}{\partial x}\right]^2 = 4\mathrm{Im}^2\left\{\langle\psi(x)|\hat{E}(\xi)\left[\hat{h}(x) - g(x)\right]|\psi(x)\rangle\right\}$$
$$\leqslant 4\left|\langle\psi(x)|\hat{E}^{1/2}(\xi)\hat{E}^{1/2}(\xi)\left[\hat{h}(x) - g(x)\right]|\psi(x)\rangle\right|^2$$
$$\leqslant \langle\psi(x)|\hat{E}(\xi)|\psi(x)\rangle 4\langle\psi(x)|\left[\hat{h}(x) - g(x)\right]\hat{E}(\xi)$$
$$\times \left[\hat{h}(x) - g(x)\right]|\psi(x)\rangle$$
$$= 4p(\xi|x)\langle\psi(x)|\left[\hat{h}(x) - g(x)\right]\hat{E}(\xi)$$
$$\times \left[\hat{h}(x) - g(x)\right]|\psi(x)\rangle \tag{50}$$

where in the last step the Schwarz inequality was used.

From

$$\left[\frac{\partial p(\xi|x)}{\partial x}\right] \leqslant 4p(\xi|x)\langle\psi(x)|\left[\hat{h}(x) - g(x)\right]\hat{E}(\xi)$$
$$\times \left[\hat{h}(x) - g(x)\right]|\psi(x)\rangle \tag{51}$$

one gets

$$F(x) = \int d\xi \frac{1}{p(\xi|x)}\left[\frac{\partial p(\xi|x)}{\partial x}\right]^2$$
$$\leqslant 4\int d\xi\, \langle\psi(x)|\left[\hat{h}(x) - g(x)\right]\hat{E}(\xi)\left[\hat{h}(x) - g(x)\right]|\psi(x)\rangle$$
$$= 4\langle\psi(x)|\left[\hat{h}(x) - g(x)\right]^2|\psi(x)\rangle, \tag{52}$$

or yet, in terms of the initial state $|\psi(0)\rangle$,

$$F(x) \leqslant 4\langle\psi_0| \left[\hat{H}(x) - g(x)\right]^2 |\psi_0\rangle \,,$$

$$\hat{H}(x) \equiv i\frac{d\hat{U}^\dagger(x)}{dx}\hat{U}(x) \,. \tag{53}$$

The bound attains its minimum when $g(x) = \langle\psi_0|\hat{H}(x)|\psi_0\rangle \equiv \langle\hat{H}(x)\rangle_0$. This yields the upper bound for the Fisher information,

$$F(x) \leqslant 4\langle(\Delta\hat{H})^2\rangle_0 \,,$$

$$\langle(\Delta\hat{H})^2\rangle_0 \equiv \langle\psi_0| \left[\hat{H}(x) - \langle\hat{H}(x)\rangle_0\right]^2 |\psi_0\rangle \,. \tag{54}$$

We show now that this upper bound is actually attained by a proper measurement, and therefore it coincides with the quantum Fisher information.

We consider that the outgoing state is $|\psi(x)\rangle$, and the measurement is defined by

$$\hat{E}_1 = |\psi(x_{\text{true}})\rangle\langle\psi(x_{\text{true}})| \,,$$

$$\hat{E}_2 = 1 - |\psi(x_{\text{true}})\rangle\langle\psi(x_{\text{true}})| \,, \tag{55}$$

and show that the corresponding Fisher information attains the upper bound (54). In this case,

$$F(x) = \frac{1}{p_1(x)}\left[\frac{dp_1(x)}{dx}\right]^2 + \frac{1}{p_2(x)}\left[\frac{dp_2(x)}{dx}\right]^2 \,, \tag{56}$$

$$p_1(x) = |\langle\psi(x)|\psi(x_{\text{true}})\rangle|^2 \,, \quad p_2(x) = 1 - p_1(x) \,. \tag{57}$$

Therefore,

$$F(x) = \frac{1}{p_1(x)[1 - p_1(x)]}\left[\frac{dp_1(x)}{dx}\right]^2 \,. \tag{58}$$

Since $\lim_{x\to x_{\text{true}}} p_1(x) = 1$ and $\lim_{x\to x_{\text{true}}}[dp_1(x)/dx] = 0$, this expression is indeterminate when $x = x_{\text{true}}$. Using l'Hôpital's rule, one gets

$$\lim_{x\to x_{\text{true}}} F(x) = -2\left[\frac{d^2p_1(x)}{dx^2}\right]_{x\to x_{\text{true}}}$$

$$= 4\langle\psi_0|(\Delta\hat{H})^2|\psi_0\rangle\Big|_{x=x_{\text{true}}} \,, \tag{59}$$
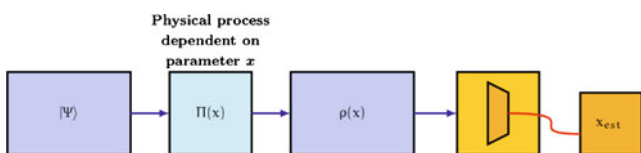
Fig. 3 (Color online) Quantum parameter estimation. The probe is prepared in an initial state $|\Psi\rangle$, the physical process is described in general by a set of Kraus operators $\Pi(x)$ that depend on the parameter to be estimated. The estimated value of the parameter, x_{est}, is obtained from the results of the measurement made on the final state of the probe, $\rho(x)$

where, as before, $\hat{H}(x) \equiv i\frac{d\hat{U}^\dagger(x)}{dx}\hat{U}(x)$. This is precisely the upper bound (54) found before. This shows that the upper bound (54) is attainable, and it must therefore coincide with the quantum Fisher information (Fig. 3). Also, from this derivation, it is seen that the measurement defined by (55), which corresponds to projecting onto the true final state and its complement, leads to the maximization of the Fisher information. This proves that, for pure states, the quantum Fisher information is given by (45) and (46).

6 Examples of the Quantum Cramér–Rao Uncertainty Relation

This section discusses a few examples, to illustrate the concepts developed in Section 5.

6.1 Spatial Displacement and Momentum

The parameter we want to estimate may be a displacement, as in Fig. 4. We have a system that is displaced by X and we know that displacements are generated by the operator $\hat{P}$, the momentum of the system. In order words, the state $|\psi(X)\rangle$ is related to $|\psi_0\rangle$ by the unitary operator $e^{iX\hat{P}/\hbar}$:

$$|\psi(X)\rangle = e^{iX\hat{P}/\hbar}|\psi_0\rangle \,. \tag{60}$$

The unitary operator $\hat{U}(X)$ defined in Section 5 is therefore $e^{iX\hat{P}/\hbar}$, and so we can find the operator $\hat{H}$ from (43), which yields

$$\hat{H} = \frac{\hat{P}}{\hbar} \,. \tag{61}$$

We now recall that $\mathcal{F}_Q$ is the variance of $\hat{H}$, to write the following expression for the quantum Fisher information:

$$\mathcal{F}_Q(X) = \frac{4\langle(\Delta\hat{P})^2\rangle_0}{\hbar^2} \,. \tag{62}$$

From (62), we are led to the Cramér–Rao relation, which tells us that the variance of the standard deviation of X_{est} with respect to the true value of the displacement
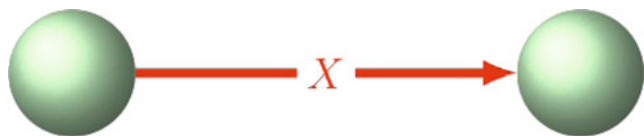
Fig. 4 (Color online) Measurement of a displacement. The quantum Cramér–Rao bound allows the derivation of a lower bound for the uncertainty in the estimation of the displacement X of a system

X, for an unbiased estimator, is bounded by the inverse of the Fisher information:

$$\langle (\delta X)^2 \rangle \geqslant \frac{\hbar^2}{4\nu \langle (\Delta \hat{P})^2 \rangle_0} . \tag{63}$$

This result relates the momentum to the uncertainty in the determination of a spatial displacement and also takes into account the number of repetitions. As mentioned before, one should distinguish (63) from the usual Heisenberg relation. Here, X is a parameter, not an operator, and the factor ν is not found in the standard Heisenberg relation.

6.2 Phase of the Harmonic Oscillator

To examine a more complex example, we consider now the relation between the uncertainty of the phase of the harmonic oscillator and the variance of the number operator. We know that shifts in the phase ϕ of the oscillator are generated by the number operator $\hat{n} = \hat{a}^\dagger \hat{a}$.

Indeed, if we start with a state $|\psi_0\rangle$, represented by the golden circle in Fig. 5, and apply the operator $\exp(i\phi\hat{n})$, we get the rotated state

$$|\psi(\phi)\rangle = \exp(i\phi\hat{n})|\psi_0\rangle, \tag{64}$$

represented by the red circle in the figure. For $\phi = \omega t$, this is just the usual free evolution of a harmonic oscillator.

Equation (64) defines a generator of rotations for the harmonic oscillator. The operator in (43) is, in the present case, $\hat{H} = \hat{n}$. The Cramér–Rao bound has, therefore, the form

$$\langle (\delta\phi)^2 \rangle \langle (\Delta\hat{n})^2 \rangle \geqslant \frac{1}{4\nu}, \tag{65}$$
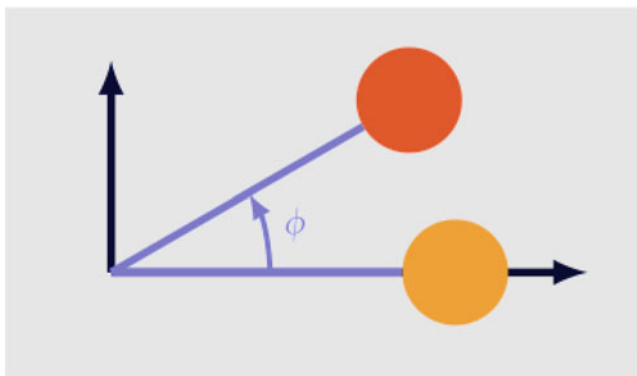

Fig. 5 (Color online) Rotation in phase space of a harmonic-oscillator state

an equality relating the variance in the phase displacement, for unbiased estimators, with the variance in the number of photons in an optical state, for instance.

An objection may be raised against (65). If the initial state $|\psi(0)\rangle$ is a Fock state, then the variance in the number of photons is zero, and the resulting phase variance would be infinite, $\langle (\delta\phi)^2 \rangle = \infty$. That would seem inadmissable, since the phase is defined in the interval $0 \leqslant \phi < 2\pi$.

The solution to this apparent paradox comes from (19), which in this case reads

$$\delta\phi = \frac{\phi_{est}}{|d\langle\phi_{est}\rangle_\phi/d\phi|} - \phi. \tag{66}$$

Since the phase of a Fock state can always be gauged away, the average $\langle\phi_{est}\rangle_\phi$ is independent of ϕ. The derivative in the denominator of the first term on the right-hand side of (66) is zero and hence $\delta\phi$ is infinite. Fock states are therefore consistent with (65), as long as one adopts biased estimators as suggested by (66).

6.3 Time and Energy

Consider a state that evolves according to the expression

$$|\psi(T)\rangle = \exp(-iT\hat{H}/\hbar)|\psi(0)\rangle, \tag{67}$$

where $\hat{H}$ is now the time independent Hamiltonian for our system, and T is the elapsed time. We again apply the Cramér–Rao bound to find the expression

$$\langle (\delta T)^2 \rangle \langle (\Delta H)^2 \rangle \geqslant \frac{\hbar^2}{4\nu}, \tag{68}$$

where $\langle (\delta T)^2 \rangle$ is the mean square deviation of the estimator from the actually elapsed time T. The uncertainty in the elapsed time is inversely proportional to the energy dispersion.

One could not possibly interpret (68) as a standard Heisenberg uncertainty relation, since there is no Hermitian operator associated with time. Equation (68) is an example of the so-called "generalized Heisenberg relation" [7], an inequality linking the energy dispersion to the uncertainty in the elapsed time—a parameter.

6.4 Optical Interferometry Revisited

For yet another application of the formalism in Section 5, we examine now the optical interferometer in Fig. 1 from a different viewpoint. Section 2 showed that the NOON states are more sensitive to a phase displacement than the coherent states. The analysis in

Section 6.2 shows that the Fisher information is proportional to the square of the variance in the number of photons in the upper arm,

$$\mathcal{F}_Q(\theta) = 4\langle(\Delta\hat{n})^2\rangle_0, \tag{69}$$

the index zero indicating that the average is taken in the initial state.

With coherent states, we are led to the standard limit, simply because the standard deviation for coherent states is proportional to the average number of photons,

$$4\langle(\Delta\hat{n})^2\rangle = 4\langle\hat{n}\rangle, \tag{70}$$

Introducing this result into the Cramér–Rao relation, we can see that the uncertainty in the phase is inversely proportional to the square root of the average number of photons in the upper arm:

$$\delta\theta \geqslant \frac{1}{2\sqrt{\langle\hat{n}\rangle_0}}. \tag{71}$$

We want to push the bound on the right-hand side downward. To that end, according to (69), we should maximize the variance of $\Delta\hat{n}$. The NOON state, defined by (26), does maximizes the variance, since it is a linear combination of two states, one with N photons in the upper arm, the other with zero photons. The variance is now

$$\langle(\Delta\hat{n})^2\rangle_0 = \frac{N^2}{4}, \tag{72}$$

which yields a phase uncertainty inversely proportional to N:

$$\delta\theta \geqslant \frac{1}{N}, \tag{73}$$

a bound that, for large N, is much less restrictive than the one in (71). Again, we conclude that the NOON states offer better precision for the same amount of resources.

7 Parameter Estimation with Decoherence

Decoherence changes the entire picture (Fig. 6). First, let us understand why it is deleterious. We have just seen that the NOON state in (26) corresponds to optimal sensitivity. If a single photon is lost, however, we only have to detect the emission of that photon to identify the arm that had N photons, for the arm with no photons cannot emit light. Thus, if a single photon is lost from the upper arm, the NOON state collapses into the state

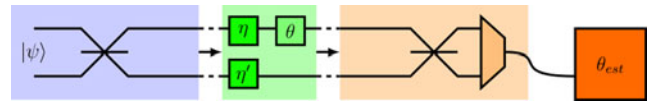$$|\psi_U(N-1)\rangle = |N-1, 0\rangle. \tag{74}$$

Fig. 6 (Color online) Optical interferometer with photon absorption. The aim is to estimate the phase θ in a Mach–Zehnder interferometer. The photon losses in the upper and lower arms are parametrized by the parameters η and η', respectively, which are equal to zero for total loss, and to one when there is no loss

Likewise, if a single photon is lost from the lower arm, it collapses into the state

$$|\psi_L(N-1)\rangle = |0, N-1\rangle. \tag{75}$$

Loss of a single photon is sufficient to destroy entanglement, and of course neither of the states in (74) and (75) is sensitive to phase, since the sensitivity of the NOON states stems from the different phase factors on the right-hand side of (27). We want probes that are robust against photon loss, which rules out the NOON states (Fig. 6).

7.1 Experimental Results on Two-Photon Interferometry

It is only natural to wonder, at this point, whether any robust state can be constructed to yield better precision than coherent states. This question has been discussed in the literature, and a particularly instructive answer was recently published [22].

Kacprowicz et al. [22] considered two-photon states. In the absence of decoherence, the best state would be a linear combination of $|2, 0\rangle$ with $|0, 2\rangle$, an entangled state. Figure 7 shows the experiment. We see a Mach–
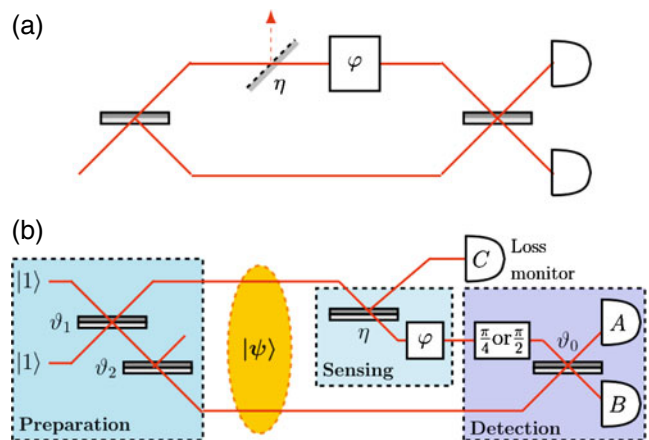

Fig. 7 (Color online) The experiment reported in [22]. A beam splitter inserted in the upper arm simulates losses under controllable conditions. The beam splitters ϑ_1 and ϑ_2 prepare the probe state. Schematic reproduction of Fig. 1 in [22]

Zehnder interferometer and, in the upper arm, the phase φ to be evaluated. Also in the upper arm, a beam splitter has been introduced, with transmissivity η, to simulate losses under controllable conditions. The parameter η can range from zero to unity.

Following the general method proposed in [23] for obtaining the best states in the presence of noise, the authors considered states of the form

$$|\psi\rangle = \sqrt{x_2}|2, 0\rangle + \sqrt{x_1}|1, 1\rangle - \sqrt{x_0}|0, 2\rangle, \qquad (76)$$

with coefficients x_0, x_1, and x_2 that must be determined for each amount of loss. The state $|\psi\rangle$ in (76) is more robust than the NOON state, because the component $|1, 1\rangle$ ensures entanglement to survive the loss of a photon.

As indicated by Fig. 7b, the preparation stage of the experiment involves two beam splitters. A pair of photons is sent through the first splitter. As it was established in the famous Hong–Ou–Mandel experiment, if twin photons come to a 50–50% transmission beam splitter simultaneously and with the same polarization, then the two photons follow either the upper or the lower red line in the figure. There is no chance that one of the photons takes the upper route while the other takes the lower one. Thus, the first beam splitter prepares a two-photon NOON state.

Here, however, the authors wanted the state in (76), not a NOON state. They therefore started with a beam splitter ϑ_1 with a different transmittance, not 50–50%, which forces a $|11\rangle$ component to arise. A second beam splitter ϑ_2 then adjusts the components x_i ($i = 1, 2, 3$).

Following the preparation stage, the state crosses the interferometer in the central section of Fig. 7b, with a lossy beam splitter, and the photons are then detected.

Figure 8 shows a theoretical result comparing the uncertainty in the phase for three states: $|\psi\rangle$ given by (76), the NOON state, and a coherent state, labeled SQL to remind us that it corresponds to the standard quantum limit. The horizontal axis represents the losses. The parameter η goes from zero (no transmission) to unity (no losses, or 100% beam splitter transmission). If there are no losses, $|\psi\rangle$ coincides with a NOON state, that is, the phase uncertainties are equal. As soon as there are losses, the precision associated with the NOON state, which is very sensitive to noise, deteriorates rapidly and soon becomes worse than that of a coherent state. By contrast, the intermediate state $|\psi\rangle$ leads to a phase uncertainty better than the standard quantum limit for all $\eta > 0$. In fact, the solid curve is always below the standard quantum limit, to which it converges as the losses become substantial.
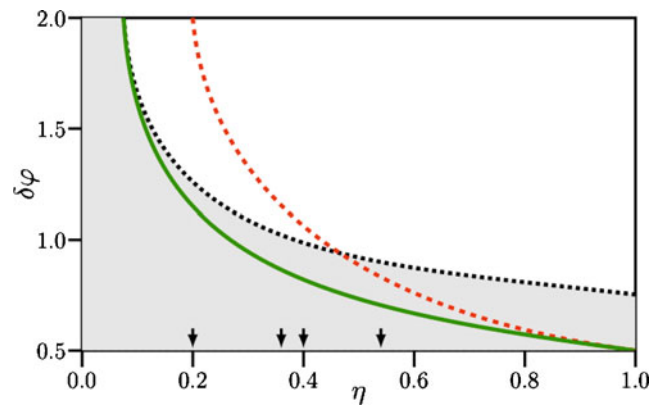

Fig. 8 (Color online) Optimal two-photon states for phase estimation. The *solid curve* corresponds to the optimal state for η, which parametrizes the losses. The dashed curve corresponds to the NOON state. The *dotted curve* bounding the *gray* region corresponds to the standard quantum limit. The four *vertical arrows* point to the η's labeling the four panels in Fig. 9. Schematic reproduction of Fig. 2 in [22]

The theoretical results in Fig. 8 find echo in the experimental data. Figure 9 shows the phase uncertainties for four different values of η, corresponding to the four points marked by the vertical arrows pointing to the horizontal axis in Fig. 8. For $\eta = 0.2$, for instance, the first panel in Fig. 8 shows that $\delta\varphi$ associated with the NOON state is nearly 2, while the $|\psi\rangle$ state and the standard quantum limit practically coincide. Four points are shown for each η, which correspond to four different phases φ. As we move across Fig. 9, the losses diminish and we see that $|\psi\rangle$ does always better than the standard quantum limit and the NOON state. This experiment was a proof of principle showing that, with decoherence, the best states lie between the coherent state and the states that optimize precision in the absence of decoherence.

These results motivate important questions regarding the behavior of the precision as the number of
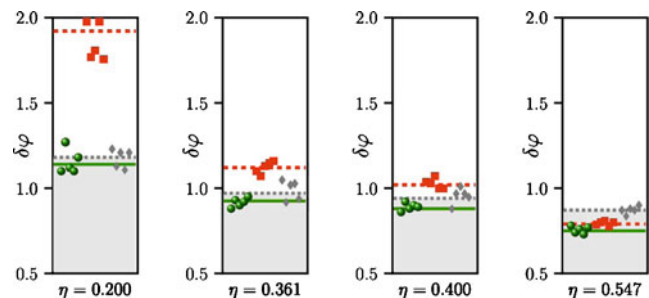

Fig. 9 (Color online) Experimentally determined uncertainties of phase estimates. The *spheres* correspond to the optimal state for each loss parameter η. The *squares* and *diamonds* correspond to the NOON states and standard limit, respectively. For larger losses (small η), the NOON states lead to bad phase estimates. Schematic reproduction of Fig. 5 in [22]

photons increases. The approach developed in [23], based on numerical calculation of the best photonic states, becomes quite cumbersome for large photon numbers. In the following, we present a new approach that leads to useful analytical bounds for the precision, thus avoiding demanding numerical procedures.

7.2 General Approach to Quantum Parameter Estimation

Compare the analyses in Sections 5 and 6 with the treatment in Section 7.1. For pure states, the Fisher information is proportional to the variance of an operator defined by unitary evolution, a very simple result. For a mixed state in a noisy system, by contrast, the procedure in Section 7.1 relies on numerical calculations that become more and more complex as N increases. We will now discuss an alternative, more general approach [16].

Figure 10 depicts the starting point of our analysis. The central region represents a noisy system that depends on a parameter that we want to estimate. The external region describes a reservoir, to which the system is coupled. Although the evolution of the noisy system is non-unitary, the dynamics of the set comprising the system and the reservoir is unitary. We turn, therefore, our attention to this larger set.

This does not mean, necessarily, that we take the physical reservoir into account. We simply define a larger state, comprising system and environment, with unitary evolution. When the environment states are traced out, we go back to the noisy evolution. The choice of the enlarged state is immaterial as long as the evolution of our system is not affected.

Thus, given an initial state

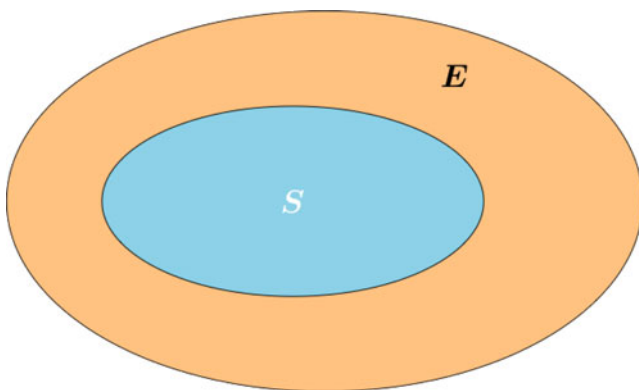$$\hat{\rho}_0 = |\psi\rangle\langle\psi|, \tag{77}$$

Fig. 10 (Color online) Schematic representation of a system in contact with an environment

we know that it will evolve according to the expression

$$\hat{\rho}(x) = \sum_\ell \hat{\Pi}_\ell(x)\hat{\rho}_0\hat{\Pi}_\ell^\dagger(x), \tag{78}$$

where the $\hat{\Pi}_\ell(x)$ are x-dependent Kraus operators.

In the enlarged system–environment state $S + E$, a enlarged state $|\Psi\rangle$ evolves as

$$|\Psi(x)\rangle = \sum_\ell \hat{\Pi}_\ell(x)|\psi\rangle_S|\ell\rangle_E, \tag{79}$$

where $|\psi\rangle_S$ is the initial state of our system, $|\ell\rangle_E$ belongs to the environment, and we are summing over a complete set of environment states. Indeed, by taking the trace of the density operator corresponding to the state $|\Psi(x)\rangle$ with respect to the environment degrees of freedom, one recovers (78). One can show that the evolution is unitary: it preserves the norm of $|\Psi\rangle$. We can hence define a unitary operator $\hat{U}_{S,E}$ by the equality

$$|\Psi(x)\rangle = \hat{U}_{S,E}(x)|\psi\rangle_S|0\rangle_E. \tag{80}$$

From (79) and (80), we have the following relation between the Kraus operators and the unitary operator $\hat{U}_{S,E}$:

$$\hat{\Pi}_\ell(x) = {}_E\langle\ell|\hat{U}_{S,E}(x)|0\rangle_E. \tag{81}$$

To be more specific, let us recapitulate the basic steps in our approach. We start with a system S and consider it along with the environment E. We then trace out the states $|\ell\rangle_E$ and are left with the evolution of a noisy system. We are free, of course, to choose the environment basis $|\ell\rangle$. Different basis will be related to each other by unitary transformations. There are hence several groups of Kraus operators associated with the same environment. In addition, different environments can lead to the same non-unitary evolution of the system, which further increases the set of allowed Kraus operators. In principle, the evolution of these different environments could also depend on the parameter x.

Consider now, in this context, the quantum Fisher information, defined before as the maximum over all possible measurements on the system of the Fisher information computed according to the classical prescription. The quantum Fisher information determines the minimum uncertainty in the parameter estimation, and is given by

$$\mathcal{F}_Q \equiv \max_{\hat{E}_j^{(S)}\otimes\mathbb{1}^{(E)}} F\left(\hat{E}_j^{(S)} \otimes \mathbb{1}^{(E)}\right). \tag{82}$$

Since it is maximized over all measurements made on the system, $\mathcal{F}_Q$ should be smaller or equal to the

maximization over all possible measurements made on the system plus environment, that is,

$$\mathcal{F}_Q \leq \max_{\hat{E}_j^{(S,E)}} F\left(\hat{E}_j^{(S,E)}\right), \tag{83}$$

because the additional freedom offered by the environment should, in principle, increase the quantum Fisher information. We therefore define the bound

$$\mathcal{C}_Q \equiv \max_{\hat{E}_j^{(S,E)}} F\left(\hat{E}_j^{(S,E)}\right). \tag{84}$$

To compute $\mathcal{C}_Q$ amounts to evaluating the quantum Fisher information for the enlarged system, which follows a unitary evolution. We can thus use the expressions derived before for this case, which express the Fisher information in terms of the variance of the generator of the unitary evolution operator, leading to

$$\mathcal{C}_Q\left(\hat{\rho}_0, \{\hat{\Pi}_\ell(x)\}\right) = 4\left[\langle \hat{H}_1(x)\rangle_0 - \langle \hat{H}_2(x)\rangle_0^2\right], \tag{85}$$

where, using (81), the generators $\hat{H}_1$ and $\hat{H}_2$ are given by:

$$\hat{H}_1(x) = \sum_\ell \frac{d\hat{\Pi}^\dagger(x)}{dx}, \frac{d\hat{\Pi}(x)}{dx} \tag{86a}$$

$$\hat{H}_2(x) = i\sum_\ell \frac{d\hat{\Pi}^\dagger(x)}{dx}\Pi(x). \tag{86b}$$

Equations (85) and (86) offer a closed expression for the bound $\mathcal{C}_Q$. It can be shown that the bound is attainable [16]: we can always choose a set of Kraus operators so that $\mathcal{C}_Q = \mathcal{F}_Q$.

In practice, minimizing $\mathcal{C}_Q$ over all Kraus operators is a difficult problem. The physical meaning of $\mathcal{C}_Q$ is given by (84): it is the information about the parameter obtained as $S + E$ is monitored. Consider, as an example, an optical interferometer, out of which photons may leak. If we detect the photons that escape into the environment after they undergo the phase shift, then we recover the information about the system parameter carried by the photon.

The fact that the bound is attainable has an interesting physical implication. When it is attainable, monitoring environment plus system becomes equivalent to monitoring only the system. In other words, monitoring $S + E$ yields the same information on the parameter x as monitoring S. Obviously, in this case the environment has only redundant information about the parameter.

8 Ultimate Precision Limits for Noisy Optical Interferometry

Let us examine in more detail the lossy optical interferometer. For simplicity, let us consider that the losses are restricted to the upper arm (Fig. 11), which corresponds to the experiment in [22].

To describe this system, we may use the master equation

$$\frac{d\hat{\rho}(t)}{dt} = -i\omega[\hat{n}, \hat{\rho}(t)] + \gamma\left[\hat{a}\,\hat{\rho}(t)\hat{a}^\dagger - \frac{1}{2}\left[\hat{n}, \hat{\rho}(t)\right]\right], \tag{87}$$

where $n = \hat{a}^\dagger\hat{a}$ is the photon number operator. The first term on the right-hand side is the free evolution of the state, since $\omega\hat{n}$ is the harmonic-oscillator Hamiltonian for the electromagnetic field mode in that arm, and the second term is the usual dissipative part of the master equation describing losses in a zero-temperature bath.

8.1 Lossy Optical Interferometry and Kraus Operators

The Kraus operators offer an alternative description. The time evolution of the density operator can be computed from the expression

$$\hat{\rho}(t) = \sum_\ell \hat{\Pi}_\ell(t)\hat{\rho}(0)\hat{\Pi}_\ell^\dagger(t). \tag{88}$$

Differentiation of both sides with respect to the time t should yield the master (87). This requirement is insufficient to uniquely identify the Kraus operators, which allows us to make sensible choices aiming to minimize the bound given by (85) and (86).

A possible model for photon loss is a beam splitter. This device was actually used in the experiment described in Section 7.1, in order to simulate the losses in a controllable way.

A detailed analysis of the quantum mechanics of a beam splitter is useful at this point, since it leads to the explicit construction of a simple set of Kraus operators. Suppose a Fock state $|\Psi_{in}^{(a)}\rangle = |n\rangle$ is incident on the beam splitter shown in Fig. 12. This can be considered as the initial state of the horizontally propagating mode a. The initial state of the vertical mode b is the vac-
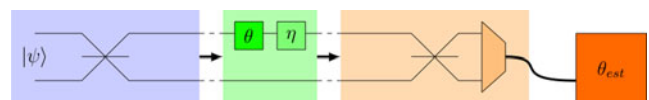

Fig. 11 (Color online) Optical interferometer with losses in the upper arm. The phase shift θ arises from an inserted dispersive medium or from unbalancing the interferometer. The losses are parametrized by η, which ranges from $\eta = 0$ (full loss) to $\eta = 1$ (no losses)
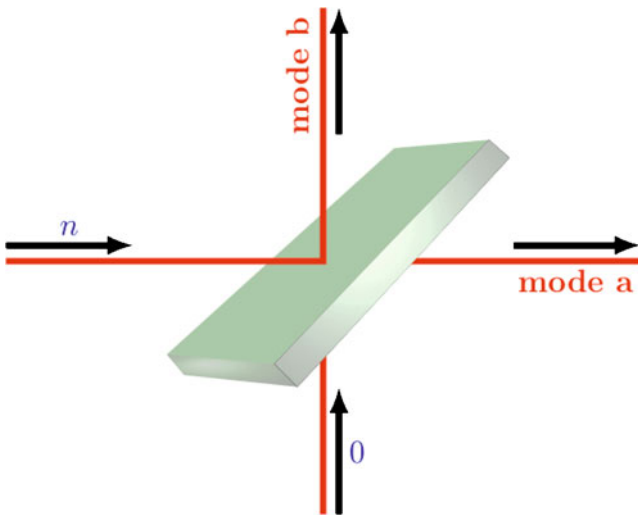
Fig. 12 (Color online) Beam splitter as a model for the photon-loss mechanism. Out of n photons incident on one of the ports of the beam splitter, a fraction is transmitted, the remainder being reflected into mode b

uum $|0\rangle$, since no photons are incident in this mode. Therefore, the initial state of the two modes can be written as $|\Psi_{in}\rangle = |n, 0\rangle$, the first argument standing for mode a, the second for mode b. Let $t = \sqrt{\eta}$ be the transmissivity of the beam splitter, and $r = \sqrt{1 - t^2}$ its reflectivity, both assumed to be real for simplicity. Then the outgoing state can be written as

$$|\Psi_{out}\rangle = \sum_{\ell=0}^{n} \binom{n}{\ell}^{1/2} r^\ell t^{n-\ell} |n - \ell, \ell\rangle, \tag{89}$$

an expression that has a clear physical meaning. Indeed, it implies that the probability that ℓ photons are reflected and $n - \ell$ are transmitted is

$$P(n - \ell, \ell) = \binom{n}{\ell} r^{2\ell} t^{2(n-\ell)}, \tag{90}$$

a result easily derived from combinatorial analysis, since r^2 is the probability that a single photon is reflected into mode b and the combinatorial factor is the number of ways ℓ photons can be reflected from the initial n photons incident on the beam splitter.

If now

$$|\Psi_{in}\rangle = \left(\sum_{n=0}^{\infty} a_n |n\rangle_a \right) \otimes |0\rangle_b, \tag{91}$$

the reduced density operator corresponding to the outgoing state in mode a can be easily calculated from the above expressions, yielding

$$\rho_{out}^{(a)}(\eta) = \sum_{\ell=0}^{\infty} \hat{\Pi}_\ell(\eta) \left| \Psi_{in}^{(a)} \right\rangle \left\langle \Psi_{in}^{(a)} \right| \hat{\Pi}_\ell^\dagger(\eta), \tag{92}$$

where

$$\hat{\Pi}_\ell(\eta) = \sqrt{\frac{(1 - \eta)^\ell}{\ell!}} \eta^{\hat{n}/2} \hat{a}^\ell. \tag{93}$$

This is a Kraus operator representation of the lossy evolution of the field in mode a, still without considering the phase shift. If we set $\eta = \exp(-\gamma t)$, where γ is the loss rate and t is the transit time through the upper arm, and differentiate (92) with respect to time, we get the loss term in the master (87).

The Kraus operators for the optical interferometer should also include a phase factor $e^{i\hat{n}\theta}$ to account for the phase displacement of the $N - \ell$ photons crossing the dispersive medium. The Kraus operator has hence the form

$$\hat{\Pi}_\ell(\theta, \eta) = \sqrt{\frac{(1 - \eta)^\ell}{\ell!}} e^{i\theta\hat{n}} \eta^{\hat{n}/2} \hat{a}^\ell, \tag{94}$$

where the operators on the right-hand side have been ordered to describe the arrangement in Fig. 13a, in which the photons are lost before the phase is displaced.

If the environment in Fig. 13a is measured, information is partially recovered. The environment has no information about the phase, because the photons were reflected before crossing the dispersive medium, but it keeps track of the number of lost photons.

Alternatively, we can place the beam splitter after the phase displacement, as in Fig. 13b. In the expression for the Kraus operator, the phase now appears to the right of the annihilation operator,

$$\hat{\Pi}_\ell(\theta, \eta) = \sqrt{\frac{(1 - \eta)^\ell}{\ell!}} \eta^{\frac{\hat{n}}{2}} \hat{a}^\ell e^{i\theta\hat{n}} \tag{95}$$
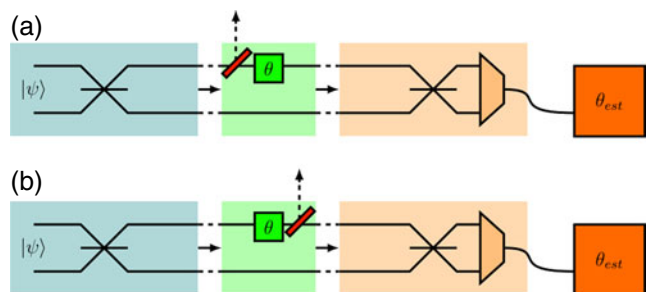

Fig. 13 (Color online) Optical interferometer with losses in the upper arm. Two different loss models are shown, corresponding to placing a beam splitter before or after the phase shift θ, which may be associated for instance with a dispersive element inserted in the upper arm

The commutation relation between $\hat{a}$ and $\hat{n}$ allows us to bring (95) to the form

$$\hat{\Pi}_\ell(\theta, \eta) = \sqrt{\frac{(1-\eta)^\ell}{\ell!}} e^{i\theta(\hat{n}+\ell)} \eta^{\frac{\hat{n}}{2}} \hat{a}^\ell, \qquad (96)$$

which can be compared with (94). The right-hand sides are distinct because the exponents of the second factors on the right-hand sides differ by $i\theta\ell$. And if we measure the environment, along with the system, in the arrangement of Fig. 13b, we have full recovery of information, because the photons were scattered off the system after probing the phase. If they are measured along with the photons that go through the beam splitter, information is fully recovered.

Equations (94) and (96) can be combined into a single expression with the general form

$$\hat{\Pi}_\ell(\theta, \eta; \alpha) = \sqrt{\frac{(1-\eta)^\ell}{\ell!}} e^{i\theta(\hat{n}-\alpha\ell)} \eta^{\frac{\hat{n}}{2}} \hat{a}^\ell. \qquad (97)$$

With $\alpha = 0$, we recover (94), and with $\alpha = -1$, (96).

Equation (97) thus interpolates between the two extremes and introduces a parameter α allowing optimization. From a physical viewpoint, the interpolation seems more satisfactory than (94) or (96), for the dissipation in real systems is a sequence of events distributed throughout the dispersive medium, not an event concentrated either before or after the phase is displaced.

It is now a simple matter to compute the Hermitian operators defined by (86) and (87); we find that

$$\hat{H}_1(\theta, \eta; \alpha) = \sum_{\ell=0}^\infty \frac{(1-\eta)^\ell}{\ell!} \left(\hat{a}^\dagger\right)^\ell (\hat{n} - \alpha\ell)^2 \eta^{\hat{n}} \hat{a}^\ell, \quad (98a)$$

$$\hat{H}_2(\theta, \eta; \alpha) = \sum_{\ell=0}^\infty \frac{(1-\eta)^\ell}{\ell!} \left(\hat{a}^\dagger\right)^\ell (\hat{n} - \alpha\ell) \eta^{\hat{n}} \hat{a}^\ell. \quad (98b)$$

We can now take advantage of the commutation relation between $a^\dagger$ and $\hat{n}$ to see that

$$\left(a^\dagger\right)^\ell \hat{n} = (\hat{n} - \ell) \left(\hat{a}^\dagger\right)^\ell, \qquad (99)$$

which recasts (98) in the form

$$\hat{H}_1(\theta, \eta; \alpha) = \hat{n}^2 - 2(1+\alpha)\hat{n}\hat{S}_1(\eta)$$
$$+ (1+\alpha)^2 \hat{S}_2(\eta), \qquad (100a)$$

$$\hat{H}_2(\theta, \eta; \alpha) = \hat{n} - 2(1+\alpha)\hat{S}_1(\eta), \qquad (100b)$$

where we have defined the operators

$$\hat{S}_1(\eta) \equiv \sum_{\ell=0}^\infty \ell \frac{(1-\eta)^\ell}{\ell!} \left(a^\dagger\right)^\ell \eta^{\hat{n}} a^\ell, \qquad (101a)$$

$$\hat{S}_2(\eta) \equiv \sum_{\ell=0}^\infty \ell^2 \frac{(1-\eta)^\ell}{\ell!} \left(a^\dagger\right)^\ell \eta^{\hat{n}} a^\ell. \qquad (101b)$$

Account taken of the identity $\hat{n} \equiv \hat{a}^\dagger \hat{a}$, the sums on the right-hand sides can be carried out, and the following expressions result:

$$\hat{S}_1(\eta) = (1-\eta)\hat{n}, \qquad (102a)$$

$$\hat{S}_2(\eta) = (1-\eta)\left[\eta\hat{n} + (1-\eta)\hat{n}^2\right]. \qquad (102b)$$

Substitution on the right-hand side of (100) then shows that

$$\hat{H}_1(\theta, \eta; \alpha) = [1 - (1+\alpha)(1-\eta)]^2 \hat{n}^2$$
$$+ (1+\alpha)^2 \eta(1-\eta)\hat{n}, \qquad (103a)$$

$$\hat{H}_2(\theta, \eta; \alpha) = [1 - (1+\alpha)(1-\eta)]\hat{n}. \qquad (103b)$$

We can now substitute the right-hand side of (103a) for $\hat{H}_1$ and the right-hand side of (103b) for $\hat{H}_2$ in (85) to obtain the expression

$$\mathcal{C}_Q(\hat{\rho}_0; \alpha) = 4[1 - (1+\alpha)(1-\eta)]^2 \langle\left(\Delta\hat{n}\right)^2\rangle_0$$
$$+ 4(1+\alpha)^2 \eta(1-\eta)\langle\hat{n}\rangle_0, \qquad (104)$$

which sets an upper limit for the quantum Fisher information $\mathcal{F}_Q$, valid for all α,

$$\mathcal{F}_Q(\hat{\rho}_0) \leqslant \mathcal{C}_Q(\hat{\rho}_0; \alpha). \qquad (105)$$

In (104) and (105), $\hat{\rho}_0$ is the initial state fed into the interferometer, and $\langle\hat{n}\rangle_0$ and $\langle\left(\Delta\hat{n}\right)^2\rangle_0$ are the average of and the variance in the number of photons in the upper arm, respectively, calculated in the state $\hat{\rho}_0$.

We can now optimize the upper bound in (104). The following parameter α is easily seen to minimize $\mathcal{C}_Q$:

$$\alpha_{opt} = \frac{4\langle\left(\Delta\hat{n}\right)^2\rangle_0}{(1-\eta)\langle\left(\Delta\hat{n}\right)^2\rangle_0 + \eta\langle\hat{n}\rangle_0} - 1, \qquad (106)$$

which can be substituted on the right-hand side of (103a) to yield the optimized bound

$$\mathcal{C}_Q(\hat{\rho}_0, \alpha_{opt}) = \frac{4\eta\langle\hat{n}\rangle_0\langle\left(\Delta\hat{n}\right)^2\rangle_0}{(1-\eta)\langle\left(\Delta\hat{n}\right)^2\rangle_0 + \eta\langle\hat{n}\rangle_0}, \qquad (107)$$

a minimum restricted only by our parametrization (97) of the Kraus operators. By minimizing $\mathcal{C}_Q$, we have of course tightened the inequality in (105), which imposes an upper bound on the quantum Fisher information $\mathcal{F}_Q$.

The right-hand side of (107) has a very attractive form, because it depends on the variance of the initial state, on the number of photons in the initial state, and on the losses. We can check it in two limits. If there is small dissipation, i.e., if

$$(1 - \eta)\langle(\Delta \hat{n})^2\rangle_0 \ll \eta\langle\hat{n}\rangle_0, \tag{108}$$

the right-hand side of (107) is hence proportional to the standard deviation $\langle(\Delta \hat{n})^2\rangle$ and we recover (45), that is, we recover the quantum Fisher information for pure states.

In the opposite, highly dissipative limit

$$(1 - \eta)\langle(\Delta \hat{n})^2\rangle_0 \gg \eta\langle\hat{n}\rangle_0, \tag{109}$$

the right-hand side of (107) is now proportional to $\langle\hat{n}\rangle_0$, and the following equality follows

$$\delta\theta \geqslant \sqrt{\frac{1 - \eta}{4\eta\langle\hat{n}\rangle_0}}. \tag{110}$$

The estimation error $\delta\theta$ is therefore bounded by a number inversely proportional to the square root of the number of photons, as in the standard quantum limit.

8.2 States with Well-Defined Photon Number

Results that are easier to analyze are obtained when we examine states with fixed number of photons, such as the NOON state or the state considered in [22]. In this case, we can write

$$|\psi_0\rangle = \sum_{n=0}^{N} \beta_n |n, N - n\rangle, \tag{111}$$

and get a very simple expression for the bound [16]

$$\mathcal{C}_Q(\hat{\rho}_0, \alpha_{opt}) \leqslant \tilde{\mathcal{C}}_Q = \left[\frac{2N}{1 + \sqrt{1 + \frac{(1 - \eta)N}{\eta}}} \right]^2, \tag{112}$$

which implies the following bound for $\delta\theta$:

$$2\sqrt{\nu}\,\delta\theta \geqslant \frac{1 + \sqrt{1 + \frac{(1 - \eta)N}{\eta}}}{N}, \tag{113}$$

where ν is as before the number of experimental repetitions.

Again, we can analyze special limits for our expression. For small losses, with $N \ll \eta/(1 - \eta)$, (113) yields the Heisenberg limit

$$\sqrt{\nu}\,\delta\theta \geqslant \frac{1}{N}. \tag{114}$$

At the opposite extreme, with substantial losses, i.e., with

$$N \gg \frac{\eta}{1 - \eta}, \tag{115}$$

we have an expression that is analogous to the standard quantum limit:

$$\delta\theta \geqslant \frac{\sqrt{1 - \eta}}{2\sqrt{\nu\eta N}}. \tag{116}$$

This limit was obtained in [24] and [25] using other methods, devised specifically for calculating this asymptotic limit in optical interferometry. Our method leads instead to an analytical bound that covers the whole region of variation of the photon numbers and the loss parameter η, and is applicable to other problems, like for instance the estimation of frequencies in atomic spectroscopy in the presence of dephasing [16].

Compare now (116) with the estimation error obtained by sending N independent photons one-by-one through the interferometer—this yields the N-photon standard quantum limit. Each two-mode photon is described by the state $(|10\rangle + |01\rangle)/\sqrt{2}$. When the N-photon experiment is repeated ν times, one gets

$$\delta\theta \geqslant \frac{1 + \sqrt{\eta}}{2\sqrt{\nu\eta N}}, \tag{117}$$

easily obtained from (113) upon setting $N = 1$—since the state is now $(|10\rangle + |01\rangle)/\sqrt{2}$—and replacing ν by $N\nu$. The bound in (116) is better, but the improvement factor $\sqrt{1 - \eta}/(1 + \sqrt{\eta})$ is insufficient to bring the uncertainty to a new scale.
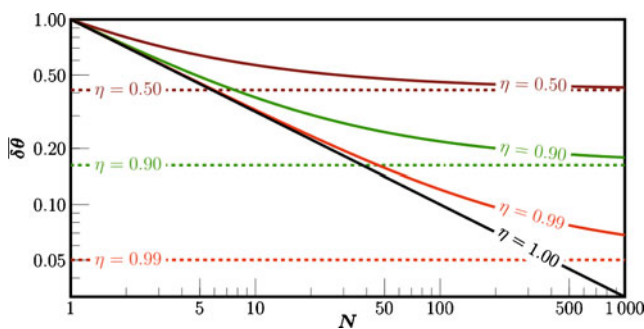

Fig. 14 (Color online) Lower bounds for the phase error as a function of the number N of photons, for the indicated loss parameters η. Shown on the vertical axis is the normalized lower bound $\overline{\delta\theta} = \delta\theta\sqrt{4\nu\eta N}/(1 + \sqrt{\eta})$, i.e., the lower bound divided by the standard quantum limit (117). The *solid straight line* represents the Heisenberg limit, which is attained in the absence of noise ($\eta = 1$). For each $\eta < 1$, a *dashed line* shows the $N \to \infty$ limit, obtained from (116)

Figure 14 shows a log–log plot of a renormalized error $\overline{\delta\theta}$, i.e., the uncertainty in the measured phase divided by the standard quantum limit, (117). In the lossless limit, $\eta = 1$, the plot coincides with the Heisenberg limit, represented by the black solid line. As dissipation rises, the plot rapidly approaches the horizontal lines representing (116), the standard quantum limit multiplied by $\sqrt{1-\eta}/(1+\sqrt{\eta})$. No matter how small the dissipation, as $N \to \infty$ the system approaches the scaling of the standard quantum limit. We can see that from (115) and (116), as well: no matter how close to unity η is, eventually N will exceed $\eta/(1-\eta)$ and $\delta\theta$ will cross over from the $1/N$ scaling, typical of the Heisenberg limit, to the standard quantum limit scaling, proportional to $1/\sqrt{N}$.

Equations (115) and (116) also show that, to maximize gain, one should work in the crossover region, where the precision still rises relatively fast as N increases, substantially faster than close to the standard quantum limit.

8.3 Tightness of the Bound

Figure 15 compares the quantum Fisher information, calculated numerically, with the bound in (112) for several values of η's and different numbers of photons, up to $N = 100$. Not surprisingly the bound is alw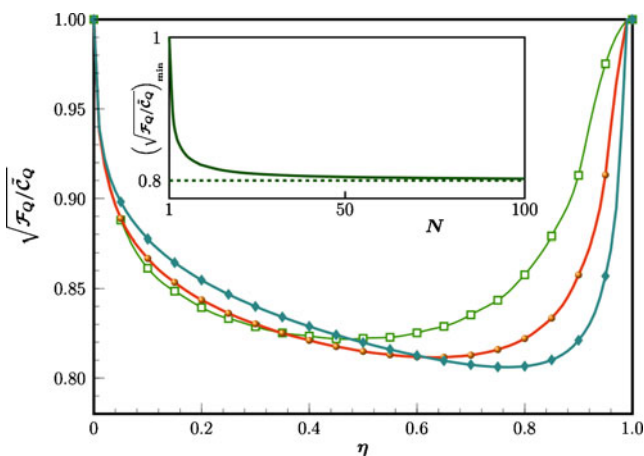ays smaller than or equal to the Fisher information, but the plot shows that, both with large and with small losses, the bound approaches $\mathcal{F}_Q$. The bound associated with moderate losses is somewhat larger than the quantum Fisher information, each plot displaying a minimum around $\sqrt{\mathcal{F}_Q/\tilde{\mathbb{C}}_Q} = 0.8$.

The inset examines the minima from another viewpoint. It shows the lowest value of $\sqrt{\mathcal{F}_Q/\tilde{\mathbb{C}}_Q}$ as a function of N for $N < 100$, for all values of η. The minimum approaches 0.8 as N grows. The numerical data thus indicate that

$$\frac{1}{\sqrt{\nu\tilde{\mathbb{C}}_Q}} \leqslant \delta\theta \leqslant \frac{1.25}{\sqrt{\nu\tilde{\mathbb{C}}_Q}}. \tag{118}$$

To position the bound in this tight interval, only physical arguments leading to a sensible expression for the Kraus operators were necessary. The simplicity of the optimization notwithstanding, the resulting bound is always very close to the Fisher information.

9 Nonlinear Estimation Strategies

Nonlinear effects have been exploited to reduce uncertainties beyond the Heisenberg $1/N$ limit. Nonlinear interactions between the atoms of Bose–Einstein condensates have been demonstrated to yield better than $1/N$ resolution in measurements of coupling constants and interaction parameters [26, 27], for instance. Duffing nonlinearities in nanomechanical oscillators offer another example of estimation uncertainties under the $1/N$ limit [28]. Kerr-like nonlinearities have led to the same conclusion [29].

10 Conclusions

The fragility of entanglement under decoherence poses a central problem for quantum metrology. As N rises, it becomes progressively more difficult to beat the standard quantum limit. We have analyzed this difficulty in the context of lossy optical interferometry. Reference [16] discusses a similar calculation for atomic spectroscopy with dephasing, i.e., the evaluation of transition frequencies of atoms, and shows that a similar strategy also establishes a very tight bound.

Among the remaining questions, two are particularly important. First, we would like to find the most robust entangled states, for a given task, in the presence of decoherence, a question that puzzles researchers of quantum metrology and quantum computing alike. Second, to find systems in which the Heisenberg limit can be attained even in the presence of decoherence. One

Fig. 15 (Color online) Numerical test of the tightness of the bound. The square root of the numerically calculated quantum Fisher information normalized by the bound in (112), as a function of the loss η for three numbers of photons: $N = 10$ (*solid line with open squares*), $N = 20$ (*solid line with spheres*), and $N = 40$ (*solid line with diamonds*). For both small and large losses, the bound approaches the quantum Fisher information. The *inset* plots the minimum of $\sqrt{\mathcal{F}_Q/\tilde{\mathbb{C}}_Q}$ as a function of N in the interval $1 \leqslant N \leqslant 100$, to show that the minimum approaches 0.8 as N grows

should also mention the still open problems of evaluating the ultimate precision limits for non-Markovian environments and the effect of noise on nonlinear estimation strategies.

References

1. R.A. Fisher, Phil. Trans. R. Soc. A **222**, 309 (1922)
2. R.A. Fisher, Proc. Camb. Phil. Soc. **22**, 700 (1925)
3. H. Cramér, *Mathematical Methods of Statistics* (Princeton University, Princeton, 1946)
4. C.R. Rao, *Linear Statistical Inference and its Applications*, 2nd edn. (Wiley, New York, 1973)
5. C.W. Helstrom, *Quantum Detection and Estimation Theory* (Academic Press, New York, 1976)
6. A.S. Holevo, *Probabilistic and Statistical Aspects of Quantum Theory* (North-Holland, Amsterdam, 1982)
7. S.L. Braunstein, C.M. Caves, Phys. Rev. Lett. **72**, 3439 (1994)
8. V. Giovannetti, S. Lloyd, L. Maccone, Science **306**, 1330 (2004)
9. L. Aolita, R. Chaves, D. Cavalcanti, A. Acin, L. Davidovich, Phys. Rev. Lett. **100**, 080501 (2008)
10. M.P. Almeida, F. de Melo, M. Hor-Meyll, A. Salles, S.P. Walborn, P.H.S. Ribeiro, L. Davidovich, Science **316**, 579 (2007)
11. D. Cavalcanti, R. Chaves, L.A.A. Davidovich, A. Acín, Phys. Rev. Let. **103**, 030502 (2009)
12. S.F. Huelga, C. Macchiavello, T. Pellizzari, A.K. Ekert, M.B. Plenio, J.I. Cirac, Phys. Rev. Lett. **79**, 3865 (1997)
13. U. Dorner, R. Demkowicz-Dobrzanski, B.J. Smith, J.S. Lundeen, W. Wasilewski, K. Banaszek, I.A. Walmsley, Phys. Rev. Lett. **102**, 040403 (2009)
14. V. Giovannetti, S. Lloyd, L. Maccone, Nat. Photon. **5**, 222 (2011)
15. L. Maccone, V. Giovannetti, Nat. Phys. advance online publication (2011)
16. B.M. Escher, R.L. de Matos Filho, L. Davidovich, Nat. Phys. **7**, 406 (2011)
17. J.J. Bollinger, W.M. Itano, D.J. Wineland, D.J. Heinzen, Phys. Rev. A **54**, R4649 (1996)
18. J.P. Dowling, Phys. Rev. A **57**, 4736 (1998)
19. K. Kraus, *States, Effects, and Operations: Fundamental Notions of Quantum Theory* (Springer, Berlin, 1983)
20. M.A. Nielsen, I.L. Chuang, *Quantum Computation and Quantum Information* (Cambridge University Press, Cambridge, 2001)
21. S.L. Braunstein, C.M. Caves, G.J. Milburn, Ann. Phys. **247**, 135 (1996)
22. M. Kacprowicz, R. Demkowicz-Dobrzanski, W. Wasilewski, K. Banaszek, I.A. Walmsley, Nat. Photon. **4**, 357 (2010)
23. R. Demkowicz-Dobrzanski, U. Dorner, B.J. Smith, J.S. Lundeen, W. Wasilewski, K. Banaszek, I.A. Walmsley, Phys. Rev. A **80**, 013825 (2009)
24. J. Kołodyński, R. Demkowicz-Dobrzanski, Phys. Rev. A **82**, 053804 (2010)
25. S. Knysh, V.N. Smelyanskiy, G.A. Durkin, Phys. Rev. A **83**, 021804 (2011)
26. S. Boixo, S.T. Flammia, C.M. Caves, J. Geremia, Phys. Rev. Lett. **98**, 090401 (2007)
27. S. Choi, B. Sundaram, Phys. Rev. A **77**, 053613 (2008)
28. M.J. Woolley, G.J. Milburn, C.M. Caves, New J. Phys. **10**, 125018 (2008)
29. A. Rivas, A. Luís, Phys. Rev. Lett. **105**, 010403 (2010)